Applied Catalysis B: Environmental 220 (2018) 462–470

Contents lists available at ScienceDirect

Applied Catalysis B: Environmental

journal homepage: www.elsevier.com/locate/apcatb

Size effect of Pt nanoparticles on the catalytic oxidation of toluene over Pt/CeO2 catalysts

Ruosi Peng[a], Shujun Li[a], Xibo Sun[a], Quanming Ren[a], Limin Chen[a,b,c], Mingli Fu[a,b,c], Junliang Wu[a,b,c], Daiqi Ye[a,b,c,*]

[a] School of Environment and Energy, South China University of Technology, Guangzhou, 510006, China
[b] Guangdong Provincial Key Laboratory of Atmospheric Environment and Pollution Control (SCUT), Guangzhou, 510006, China
[c] National Engineering Laboratory for VOCs Pollution Control Technology and Equipment, Guangzhou, 510006, China

ARTICLE INFO

Article history:
Received 7 April 2017
Received in revised form 14 July 2017
Accepted 17 July 2017
Available online 18 July 2017

Keywords:
Pt/CeO_2 catalysts
Pt size effect
Pt dispersion
Oxygen vacancies
Toluene oxidation

ABSTRACT

The present work elucidated the size effect of Pt nanoparticles on the activity of Pt/CeO_2 catalysts toward catalytic oxidation of toluene. Size-controllable Pt nanoparticles, ranging from 1.3 to 2.5 nm, were successfully loaded on CeO_2 nanorod support by the adsorption method. The structure and chemical properties of Pt/CeO_2 catalysts are much dependent on Pt particle size. As size increases, the Pt dispersion declines while more Pt-O—Ce bonds, Ce^{3+} and oxygen vacancies exist on ceria. The catalytic activity test of toluene oxidation shows that Pt/CeO_2-1.8 sample exhibits the best catalytic performance due to the balance of both Pt dispersion and oxygen vacancy concentration of ceria. Three types of TOFs values based on Pt dispersion, oxygen vacancy concentration and both of them are calculated respectively, and the result demonstrates that the reaction rate is controlled by both of the exposed Pt atom and oxygen vacancies. In addition, the Pt/CeO_2-1.8 catalyst could work properly for 120 h with various inlet toluene concentration and be completely negligible for 5 vol% water vapour at 155 °C.

1. Introduction

Volatile organic compounds (VOCs) are considered as the significant air pollutants due to their contribution to major environmental problems such as ozone and photochemical smog [1]. Recent years, several technologies of VOCs control have been investigated, of which catalytic oxidation is generally recognized as one of the most promising method with the advantages of high destructive efficiency, lower operation cost and no organic by-product [2–4]. In order to make the reaction more economically competitive, it is necessary to develop higher performance catalytic materials which could operate at lower temperature. Various catalysts have been studied for this purpose, including supported noble metals (NMs) and transition-metal oxides [5–8].

Supported noble metals, especially Pt-based materials, have been generally regarded as the most desirable catalysts for VOCs combustion [9,10]. One interesting and promising factor that may control the activity is the Pt size, and much effort has focused on it in recent years [11–17]. For example, Song et al. synthesized a series of Pt/SBA-15 catalysts with Pt particle size of 1.7-7.1 nm, and the apparent activation energy of ethane hydrogenolysis increased linearly up to a Pt particle size of ~4 nm and then remained constant [11]. Kon et al. investigated the oxidant-free dehydrogenation of alcohols over Pt/Al_2O_3 catalysts with different Pt size, and the result showed that the sample with 1.4 nm exhibited the highest activity, suggesting the low-coordinated Pt sites and metal/support interface played important roles [14]. Chen et al. studied toluene oxidation over ZSM-5 supported Pt nanoparticles ranging from 1.3 to 2.3 nm, and found that Pt-1.9/ZSM-5 had the highest activity due to the relatively higher Pt dispersion and Pt^0 proportion [17]. These investigations suggest that different Pt size could lead to various Pt dispersion, chemical state and coordination number, then strongly influencing the catalytic activity.

While, for the system that Pt particle is loaded on "active support" such as CeO_2, TiO_2, and Fe_2O_3, the size effect of Pt particle on the reaction is much different. Unlike "inert support" mentioned above, Pt size could also affect surface properties of active support due to various strength of interaction between metal and support, influencing catalytic activity. Moreover, the reaction process and active sites would be much diverse and complex [18–21]. An et al. suggested that Pt size could adjust the redox properties and O_2-activation abilities of Pt/Fe_2O_3 catalysts, and the Pt-FeO_x interface

* Corresponding author at: School of Environment and Energy, South China University of Technology, Guangzhou, 510006, China.
E-mail address: cedqye@scut.edu.com (D. Ye).

http://dx.doi.org/10.1016/j.apcatb.2017.07.048
0926-3373/

were the primary active sites for CO oxidation [19]. Li et al. proposed elementary steps of CO oxidation over Pt/TiO_2 catalysts involved chemisorption of CO on Pt atoms and chemisorption of O_2 on TiO_2 through the investigation of Pt size effect on CO oxidation [20]. Liu et al. prepared a series of Pt/CeO_2 catalysts with different Pt size and investigated the CO oxidation activity, and the results showed that the oxygen vacancies and Pt-O—Ce solid solution could accelerate the mobility of lattice oxygen and consequently affect the activity [21]. Though these researches give a good understanding for the size effect of Pt particle supported on active support, the dependence of Pt particle size distribution for VOCs oxidation is much less clear-cut as well as its active sites.

Herein, we employed a series of size-controllable Pt nanoparticles (mean size ranges from 1.3 to 2.5 nm) and then loaded them on CeO_2 with a shape of nanorod. The structure and chemical properties were characterized by X-ray diffraction (XRD), High resolution transmission electron microscopy (HRTEM), X-ray photoelectron spectroscopy (XPS), UV Raman, Temperature programmed reduction by hydrogen (H_2-TPR) and OSC (Oxygen Storage Capacity) test. Through these techniques, size effect of Pt nanoparticle on the catalytic oxidation of toluene over Pt/CeO_2 catalysts has been investigated, affording a better understanding of the nature of their catalytically active sites.

2. Experimental section

2.1. Catalysts preparation

2.1.1. Preparation of CeO_2 nanorods

All the materials used were of analytical purity. The CeO_2 support with a shape of nanorod was prepared by a hydrothermal method [22]. 5 mmol cerous acetate was dissolved in 20 ml deionized water, and then 55 ml NaOH solution (7 mol L^{-1}) was added in it. This stock solution was stirred at room temperature for 30 min and then transferred into a 100 ml Teflon-lined stainless steel autoclave. Hydrothermal treatment was carried out at 130 °C for 5 h. After the reaction was completed, the obtained solid product was washed with deionized water and ethanol sever times and then dried at 70 °C for 12 h.

2.1.2. Synthesis of Pt nanoparticles

A series of Pt nanoparticles with mean diameters from 1.3 to 2.5 nm were synthesized by a method of glycol reduction [17]. The general steps were as follows: a certain of chloroplatinic acid and 220 mg NaOH were dissolved in 50 ml glycol together with an appropriate amount of deionized water. After stirring at room temperature for 1 h, the obtained transparent yellow solution was transferred into a 100 ml three-necked flask. Then the mixed solution was heated to 90 °C quickly for 2 h with a N_2 flow passing through the reaction system, and a change in colour to dark-brown was observed without any precipitate which indicated the formation of Pt clusters. The particles were extracted from the solution by addition 0.3 mol L^{-1} HCL solution, collected by centrifugation (8000 rpm, 5 min), and dissolved in ethanol containing 40 mg PVP. The Pt nanoparticles size was controlled by the added amount of deionized water and chloroplatinic acid.

2.1.3. Synthesis of Pt/CeO_2

An appropriate amount of Pt nanocrystals (to give a final loading content of 0.25 wt%) with various size dissolved in ethanol was added to a dispersion of ceria in 20 ml ethanol. After stirring for 12 h, the solid was recovered by centrifugation (8000 rpm, 5 min) and washed twice with ethanol. Finally, the powders were dried at 70 °C overnight and calcined at 300 °C for 3 h in 5% H_2/N_2. The obtained catalysts were denoted as Pt/CeO_2-x, where x stands for the Pt nanoparticles mean diameter in parent solution.

2.2. Catalysts characterization

TEM and HRTEM images were taken in a JEM-2100HR (JEOL, Japan). The mean size of the controllable Pt nanoparticles was determined from HRTEM images of the as-prepared Pt nanoparticles. The equation was as followed:

$$d \approx \frac{\sum_i n_i d_i}{\sum_i n_i} \quad (1)$$

Where n_i is the particle number, d_i is the particles diameter.

Moreover, it is assumed that the Pt nanoparticles showed a spherical or hemispherical shape, so the dispersion of the Pt nanoparticles could be estimated based on the following equation:

$$D_{Pt} = \frac{600 M_{Pt}}{\rho d a_{Pt} N_A} \quad (2)$$

Where M_{Pt} denotes the molar weight of Pt (195.08 g mol^{-1}), ρ is the density of Pt (21.45 g cm^{-3}), d is the average particle diameter observed from the TEM images, a_{Pt} represents the surface area of Pt atom (8.06×10^{-20} m^2 $atom^{-1}$), and N_A is the Avogadro constant (6.02×10^{23} mol^{-1}).

The crystalline structure of the samples was obtained by XRD (D8 ADVANCE diffractometer Bruker, Germany) with Cu Kα radiation (40 kV, 40 mA, scanning step = 0.02°). Their chemical composition was determined by inductively coupled plasma/optical emission spectroscopy (ICP-OES, Perkin-Elmer plasma 8000). The specific surfaces area (SSA) was measured used nitrogen adsorption and desorption isotherms at 77 K on an ASAP 2020 system in static measured mode, and the Brunauer-Emmett-Teller (BET) model was used to calculate the SSA.

XPS analysis was performed using a Thermo ESCALAB 250 with Al Kα (hv = 1486.8 eV) as the excitation source. The likely charging of catalysts was corrected by setting the binding energy of the adventitious carbon (C 1s) to 284.6 eV. H_2-TPR was performed on a chemisorption analyzer (Micromeritics Chemisorb 2920II). 100 mg sample was first treated under a He flow containing 5 vol% O_2 (30 ml min^{-1}) at 300 °C for 1 h, following by purging with Ar at the same temperature for 30 min and then cooling down to room temperature. After that, a flow of 10% H_2/Ar (30 ml min^{-1}) was switched into the tube and the samples were heated up to 800 °C at a ramp of 10 °C min^{-1}.

UV Raman spectra were obtained in back-scattering configuration on a LabRAM HR Evolution Laser Raman Spectrometer (HYJ, France) with a CCD detector and a spectral resolution of 1 cm^{-1}. The Kinmon He-Cd laser (325 nm) was employed as the excitation source. The laser power on the sample was maintained at 8 mW, the spectra collected with gratings of 2400 grooves mm^{-1} and the hole was 80. The spectrum was recorded by two times 100 s subsequent laser exposer.

The concentration of surface oxygen vacancy was measured by oxygen pules injection method on the chemisorption analyzer. The experimental procedure follows previous research [23]. The consumption of oxygen by catalyst was accordingly calculated and defined as $OSC_{catalyst}$, and the consumption of oxygen by Pt was calculated based on the following definitions, which was defined as OSC_{Pt}:

$$OSC_{Pt} = 2\frac{D_{Pt} X_{Pt}}{M_{Pt}} \quad (3)$$

Where X_{Pt} is the weight fraction of Pt in the sample as determined by ICP-OES and the stoichiometric factor between oxygen and metal atom is set as 2:1. The value of surface oxygen vacancy

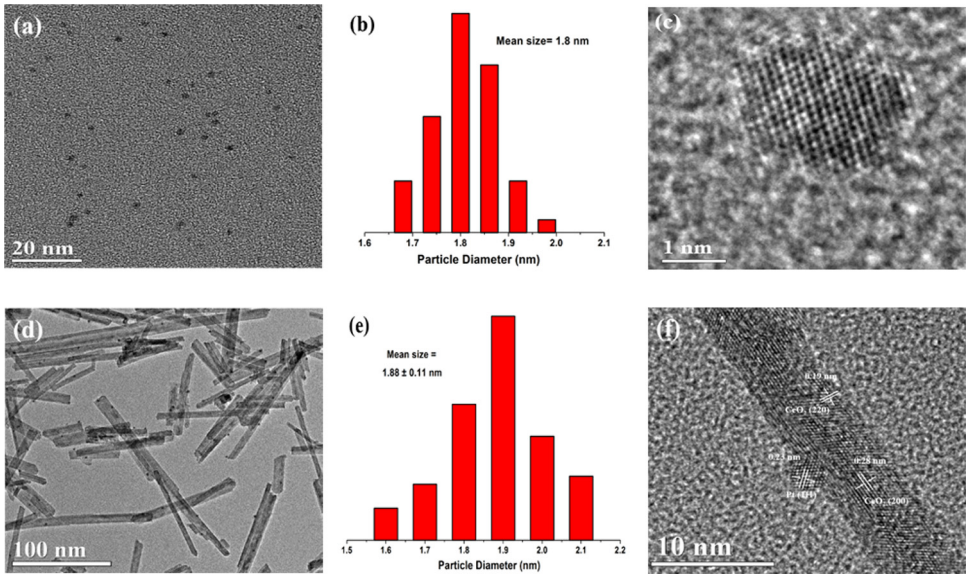

Fig. 1. TEM & HRTEM and size distribution images of the Pt nanoparticles of Pt/CeO_2-1.8 sample. (a, b and c) Pt particles in parent solution and (d, e and f) Pt particles on CeO_2 support.

concentration was denoted as $OSC_{surface}$ which is calculated by following equation:

$$OSC_{surface} = OSC_{catalyst} - OSC_{metal} \quad (4)$$

2.3. Catalytic activity test

Catalytic activities of the samples were evaluated in a continuous flow micro-reactor made quartz with 8 nm internal diameter and 50 cm length. To minimize the effect of hot spots, the sample (200 mg, 40–60 mesh) was diluted with 800 mg silicon (40–60 mesh). All the particles were packed at the bed of the reactor. The total flow rate of the reactant mixture (1000 ppm Toluene, 20% O_2/N_2) was 160 ml min^{-1}, corresponding to the weight hourly space velocity (WHSV) at 48000 ml g^{-1} h^{-1}. The reactant and product gases were analyzed by an on-line gas chromatograph (GC-2014C, Shimadzu, Japan) equipped with FID at a given temperature for 8 times after stabilizing for 15 min. Catalytic activities of the samples were evaluated using the temperature (T_{50} and T_{90}) required for achieving toluene conversions of 50% and 90%, respectively. Toluene conversion was obtained on the toluene consumption, calculated by the inlet and outlet concentration.

Three types of turnover frequencies (TOFs) were calculated based on the following equation:

$$TOF_{Pt}\left(S^{-1}\right) = X_{toluene}F_{toluene}\frac{M_{Pt}}{m_{Cat}X_{Pt}D_{Pt}} \quad (5)$$

$$TOF_{OV}\left(S^{-1}\right) = X_{toluene}F_{toluene}\frac{1}{m_{Cat}OSC_{surface}} \quad (6)$$

$$TOF_{Pt\bullet OV}\left(S^{-1}\right) = X_{toluene}F_{toluene}\frac{1}{m_{Cat}X_{Pt}D_{Pt}OSC_{surface}} \quad (7)$$

Where $X_{toulene}$ denotes the toluene conversion at certain temperature; $F_{toluene}$ is the toluene flow rate in unit of mol s^{-1}; m_{Cat} is the catalyst amount. TOF_{Pt} is the turnover frequency based on Pt dispersion; TOF_{OV} is the ty concentration on CeO_2 surface; $TOF_{Pt\bullet ov}$ is the turnover frequency based on both metal dispersion and oxygen vacancy concentration.

Activation energies were calculated at temperatures (90–110 °C) for toluene conversions lower than 10%, which was estimated using the following Arrhenius relationship.

$$\ln r = -\frac{Ea}{RT} + \ln A \quad (8)$$

Where r, A and Ea are the reaction rate (mol s^{-1}), pre-exponential factor, and apparent activation energy (kJ mol^{-1}), respectively.

2.4. Stability and H_2O resistance test

The stability of the best sample was tested with the different inlet toluene concentration at 155 °C for 120 h (1000 ppm for 60 h, 2000 ppm for 30 h and 4000 ppm for 30 h). In addition, tolerance activity of this sample at 125 °C with a lower conversion was also investigated for 40 h. Before this test, the catalyst had been treated at 300 °C for 4 h under reaction conditions (1000 ppm Toluene, 20% O_2/N_2, 48000 ml g^{-1} h^{-1}).

The effect of water vapour on the catalytic reaction was performed under the humid condition of 5% volume water, which was achieved by bubbling the water using a dry air flow at 50 °C.

3. Results and discussion

3.1. Structure analysis

The size of Pt nanoparticle and morphology of the CeO_2 support were examined by TEM and HRETM. From Fig. 1a and b and Fig.S1 (a, c, e and g), it could be found that the Pt nanoparticles in parent solution are monodispersed and the mean size is 1.3, 1.5, 1.8, 2.1 and 2.5 nm. After the loading process, the Pt particles become bigger as shown in Fig. 1d and e and Fig.S1 (b, d, f and h), probably resulting from the heating treatment. Consequently, the size increase to the values of 1.37 ± 0.09, 1.59 ± 0.12, 1.88 ± 0.11, 2.21 ± 0.14 and 2.63 ± 0.15 nm, respectively, and the corresponding dispersions are calculated by Eq. (1) and the data are summarized in Table 1. In addition, from the images of Pt/CeO_2-1.8 in Fig. 1d and f, it is observed that the CeO_2 support exhibits a shape of nanorod as expected. Their width is 8 ± 2 nm and length is distributed between 100 and 200 nm, selectively exposing (110) and (100) crystal planes. Also the lattice fringes of Pt nanoparti-

Table 1
Textural parameters of various samples.

Sample	Pt loading (%)[a]	Pt mean size (nm)[b]	Pt dispersion(%)	S_{BET}(m^2 g^{-1})[c]	Lattice parameter (nm)[d]
CeO_2	–	–	–	102.6	0.54128
Pt/CeO_2-1.3	0.22	1.37 ± 0.09	82.7 ± 5.1	97.8	0.54122
Pt/CeO_2-1.5	0.23	1.59 ± 0.12	71.2 ± 5.0	97.4	0.54121
Pt/CeO_2-1.8	0.24	1.88 ± 0.11	60.2 ± 3.3	98.7	0.54115
Pt/CeO_2-2.1	0.23	2.21 ± 0.14	51.2 ± 3.2	98.4	0.54112
Pt/CeO_2-2.5	0.23	2.63 ± 0.15	43.0 ± 2.5	99.5	0.54106

[a] Determined by ICP-OES.
[b] Determined by HRTEM.
[c] Determined from N_2 isotherm.
[d] Determined by MDI Jade 5 software.

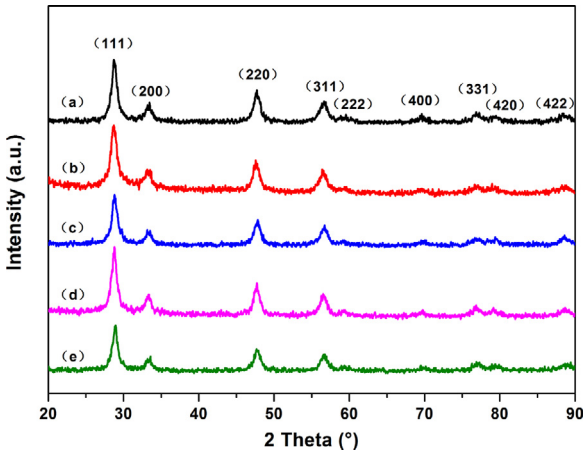

Fig. 2. XRD patterns of various Pt/CeO_2 catalysts: (a) Pt/CeO_2-1.3, (b) Pt/CeO_2-1.5, (c) Pt/CeO_2-1.8, (d) Pt/CeO_2-2.1, (e) Pt/CeO_2-2.5.

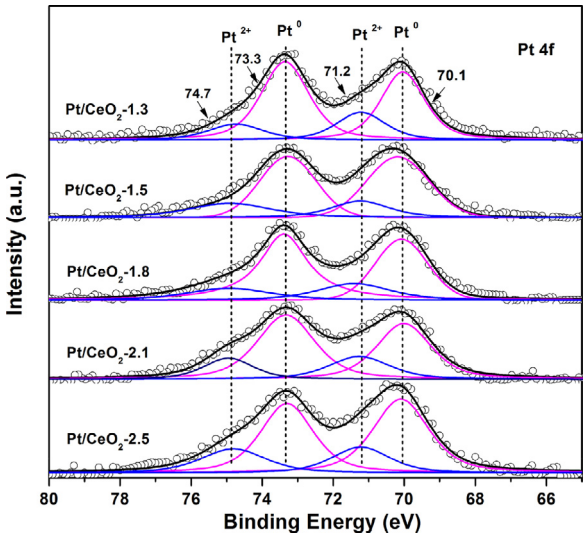

Fig. 3. XPS spectra of Pt 4f for different Pt/CeO_2 samples.

cles anchored on support could be observed clearly, and it has an interplanar distances of 0.23 nm, in consistent with the (111) plane.

The XRD patterns of Pt/CeO_2 samples with various Pt size are shown in Fig. 2. The diffraction of peaks corresponded to (111), (200), (220), (400), (311) and (420) planes are observed in all catalysts, in good agreement with the face-centred cubic fluorite structure with space group Fm–3 m (JCPDS card No. 34-0394) [22,24]. However, no diffraction peak related to Pt or PtOx phase (at around 40°) could be observed, which probably results from high dispersion of Pt species or the low loading content. As listed in Table 1, it could be found that the lattice parameter of the Pt/CeO_2 samples is smaller than that in pure CeO_2 support. The lower values indicates that partial Pt^{2+} ($r_{Pt^{2+}}$ = 0.074 nm) or Pt^{4+} ($r_{Pt^{4+}}$ = 0.076 nm) species may enter into the fluorite-like lattice CeO_2 ($r_{Ce^{4+}}$ = 0.094 nm), resulting in the shrinkage of cell and also the formation of Pt-O—Ce solid solution [21,25,26]. Moreover, it is noticeable that the decrease of lattice parameter is increasing with the Pt size, which indicates the bigger Pt nanoparticle would more easily penetrate into CeO_2 matrix. And this decline implies more Pt-O—Ce solid solution would exist in the Pt/CeO_2 samples with bigger Pt size.

In addition, the Pt loading content and surface area of Pt/CeO_2 samples were examined by ICP-OES and N_2 isotherm. Table 1 shows that the attained Pt concentration (0.22-0.24 wt%) is very close to the expected value (0.25 wt%) for each sample, confirming the effectiveness of the adsorption method for depositing platinum on a CeO_2 surface. The BET surface areas of Pt/CeO_2 samples are almost same, and the value is 97.8, 97.4, 98.7, 98.4 and 99.5 m^2 g^{-1}, respectively.

3.2. Chemical states and reduction behaviour

XPS measurements were employed to probe the chemical states of the Pt species and surface cerium species in Pt/CeO_2 catalysts. Fig. 3 presents the XPS spectra of Pt 4f. According to the literature, the Pt $4f_{7/2}$ could be deconvoluted into two peaks at 70.1 eV together with 71.2 eV, while the Pt $4f_{5/2}$ is fitted with two components at 73.3 eV and 74.7 eV [27,28]. The peaks at 70.1 eV and 73.3 eV are associated with Pt^0 species. And the peaks at 71.2 eV and 74.7 eV are attributed to Pt^{2+} species. By evaluated the compositions of different Pt species, it is found that the Pt species mainly exists in metallic states and the ratio of $Pt^0/(Pt^0 + Pt^{2+})$ is all above 70%, as shown in Table 2. Although the content of Pt^0 species shows a slight decrease with the increasing Pt size, we could still suggest these Pt/CeO_2 samples have a same Pt chemical state. For the Ce 3d spectra as shown in Fig. 4, ten peaks resulting from the pairs of spin orbit doubles can be identified through deconvolution method, according to the previous reports [29,30]. Sixth of the peaks U (900.3 eV), U″ (906.9 eV), U‴ (916.1 eV), V (881.9 eV), V″ (888.5 eV) and V‴ (897.6 eV) are characteristic of Ce^{4+}. While the other four peaks U^0 (898.6 eV), U′ (901.9 eV), V^0 (880.6 eV) and V′ (883.9 eV) could be assigned to Ce^{3+}, which is often used as an indicator for the existence of oxygen vacancies on ceria surface. Table 2 lists the Ce^{3+} content of Pt/CeO_2 samples, and it is noticeable that the amount of Ce^{3+} has a close relationship with the Pt size. The sample with bigger Pt particle size possesses higher Ce^{3+} proportion, reflecting higher concentration of oxygen vacancy. For example, the Ce^{3+} content of Pt/CeO_2-2.5 is 33.0% while the value of Pt/CeO_2-1.3 is 27.3%.

H_2-TPR measurement was used to investigate the reducibility of oxygen species in CeO_2 and Pt/CeO_2 samples, and the profiles were

Table 2
XPS and H_2-TPR data of various samples.

Sample	XPS		H_2-TPR	
	$Pt^0/(Pt^{2+}+Pt^0)$ (%)	$Ce^{3+}/(Ce^{3+}+Ce^{4+})$ (%)	Peak position (°C)	H_2 consumption(μmol g^{-1})
CeO_2	–	–	300, 428	531
Pt/CeO_2-1.3	75.1	27.3	100, 391	71.9, 436
Pt/CeO_2-1.5	74.9	28.2	99, 382	91.7, 425
Pt/CeO_2-1.8	74.0	30.9	93, 364	123.3, 484
Pt/CeO_2-2.1	72.9	32.3	95, 369	147.8, 522
Pt/CeO_2-2.5	72.2	33.0	101, 368	154.1, 495

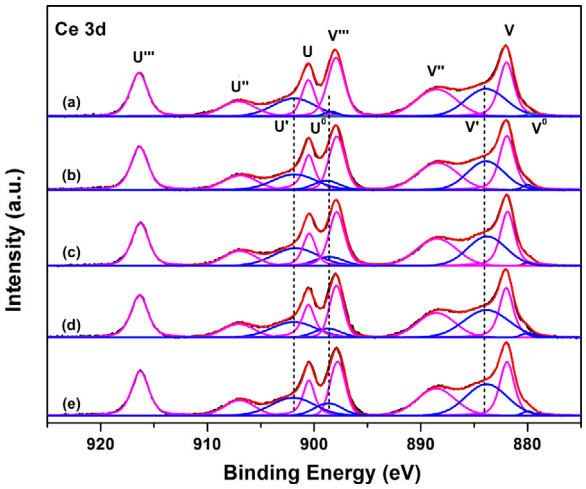

Fig. 4. XPS spectra of Ce 3d for different Pt/CeO_2 samples: (a) Pt/CeO_2-1.3, (b) Pt/CeO_2-1.5, (c) Pt/CeO_2-1.8, (d) Pt/CeO_2-2.1, (e) Pt/CeO_2-2.5.

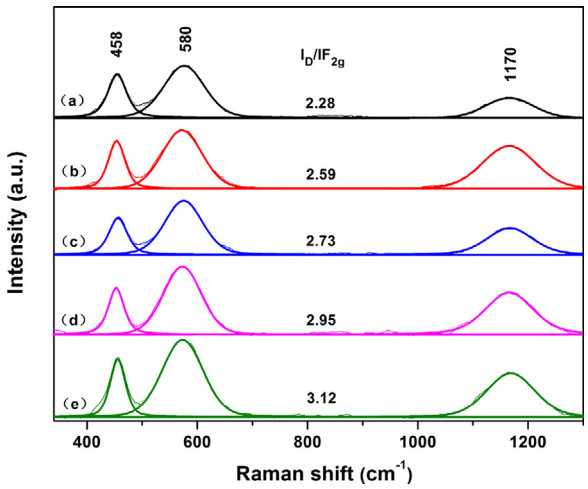

Fig. 6. Raman spectra of the Pt/CeO_2 samples: (a) Pt/CeO_2-1.3, (b) Pt/CeO_2-1.5, (c) Pt/CeO_2-1.8, (d) Pt/CeO_2-2.1, (e) Pt/CeO_2-2.5.

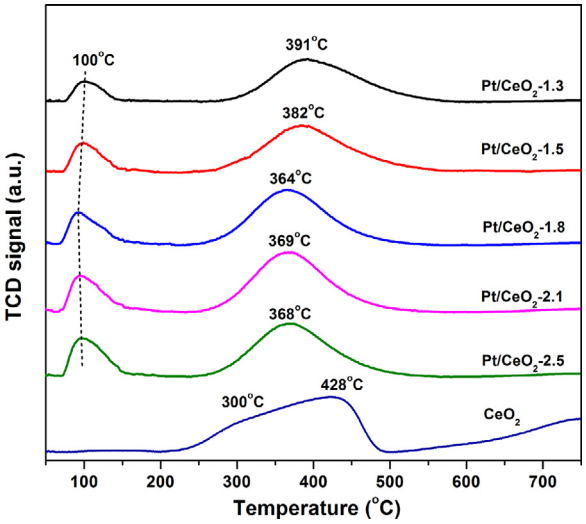

Fig. 5. H_2-TPR profiles of CeO_2 and Pt/CeO_2 samples.

shown in Fig. 5. For pure CeO_2, there is only a broad peak in range of 250–500 °C, which represents the reduction of oxygen species on surface and subsurface [22]. After the incorporation of Pt, the profile changes and two peaks could be observed. The first peak centred at about 100 °C could be assigned to the reduction of PtO_x [31]. Moreover, it is noted that the H_2 consumption of this low-temperature reduction peak for each Pt/CeO_2 sample as shown in Table 2 is much higher than the nominal value of reduction of PtO_x (about 23 μmol g^{-1}, assuming that the Pt species in the catalysts are Pt^{4+}). The extra oxygen species may come from the ceria surface/subsurface which are adjacent to Pt species due to the spillover effect induced by the metal-support interaction [21,32]. The second peak in the range of 300–500 °C could be attributed to the reduction of the surface oxygen species far away from Pt particles. Compared with the pure support, the reduction temperature of Pt/CeO_2 catalysts exhibits a significant decrease, and the appearance of the low-temperature reduction peak is probably caused by the relaxing Ce-O bond strongly bounded with Pt species [25]. This change indicates that the incorporation of Pt could activate the lattice oxygen on ceria surface/subsurface. Additionally, it could be noticeable that the H_2 consumption of this low-temperature reduction peak is closely related with the Pt size. As the Pt size becomes bigger, the H_2 consumption correspondingly increases (71.9, 91.7, 123.3, 147.8 and 154.1 μmol g^{-1} for Pt/CeO_2-1.3, Pt/CeO_2-1.5, Pt/CeO_2-1.8, Pt/CeO_2-2.1 and Pt/CeO_2-2.5, respectively), which indicates that more oxygen species on Pt/CeO_2-2.5 are reduced. From the H_2-TPR results, it could be also concluded that the Pt/CeO_2 sample with bigger Pt size would possess more Pt-O—Ce solid solution, which is in accordance with XRD results.

3.3. Concentration of surface oxygen vacancies

As an active support, the oxygen vacancies on ceria surface play a critical role in oxidation mechanism participating in the activation of gaseous oxygen and migration of active oxygen species, influencing the reaction [33–36]. In order to determine the concentration accurately, more powerful technologies UV Raman and oxygen pulse adsorption were carried out.

Fig. 6 gives the UV Raman spectra of Pt/CeO_2 samples with different Pt size. Obviously, three peaks at 458 cm^{-1}, 580 cm^{-1} and 1170 cm^{-1} could be observed. The first peak is distinguished as the symmetric stretching vibrations mode (F_{2g}) in the cubic fluorite ceria [37]. The second peak corresponds to the band of defect-induced (D) mode that connected with the oxygen vacancies induced by the existence of Ce^{3+} [38]. And the last peak

Table 3
UV-Raman spectrum and OSC data of various samples.

Sample	Raman spectral$_{D}/IF_{2g}$	OSC (μmol O g^{-1})		
		$OSC_{catalyst}$	OSC_{metal}	$OSC_{surface}$
Pt/CeO_2-1.3	2.28	90.6	18.7 ± 1.2	71.9 ± 1.2
Pt/CeO_2-1.5	2.59	102.5	16.8 ± 1.2	85.7 ± 1.2
Pt/CeO_2-1.8	2.73	145.8	14.8 ± 0.8	131.0 ± 0.8
Pt/CeO_2-2.1	2.95	148.1	11.8 ± 0.7	136.6 ± 0.7
Pt/CeO_2-2.5	3.12	157.8	10.1 ± 0.6	147.7 ± 0.6

is considered as second-order longitudinal optical (2LO) mode. Generally, the relatively intensity ratio of I_D/IF_{2g} could represent the relative oxygen vacancy concentration [39,40]. And it could be found that the I_D/IF_{2g} value of Pt/CeO_2 samples are much different and exhibit a correlation with the Pt particle size. As shown in Table 3, the value follows the sequence Pt/CeO_2-1.3 (2.28) < Pt/CeO_2-1.5 (2.59) < Pt/CeO_2-1.8 (2.73) < Pt/CeO_2-2.1 (2.95) < Pt/CeO_2-2.5 (3.12). And this suggests more oxygen vacancies would exist on surface of Pt/CeO_2 sample that has a bigger Pt size.

In order to obtain the concentration of oxygen vacancy quantificationally, OSC test was carried out. After deducting the OSC_{Pt} value from $OSC_{catalyst}$, we could obtain the $OSC_{surface}$ value that is the oxygen consumption by oxygen vacancies on ceria surface [23]. As shown in Table 3, the Pt/CeO_2-2.5 sample gives an $OSC_{surface}$ value of 147.7 ± 0.6 μmol O g^{-1}, higher than Pt/CeO_2-2.1 (136.6 ± 0.7 μmol O g^{-1}), Pt/CeO_2-1.8 (131.0 ± 0.8 μmol O g^{-1}), Pt/CeO_2-1.5 (85.7 ± 1.2 μmol O g^{-1}) and Pt/CeO_2-1.3 (71.9 ± 1.2 μmol O g^{-1}), which is in accordance with XPS and Raman data. These characterization results suggest that the concentration of oxygen vacancy on ceria is much dependent on the Pt particle size, and the bigger Pt size would give a higher concentration. In general, the various metal-support interaction, which could deeply influence the oxygen vacancy formation energy, is considered as one of the important factor to result in the different oxygen vacancy concentration of ceria-based catalysts [23,38,41,42]. Combined with the results of XRD and H_2-TPR, probably due to stronger metal-support interaction, the Pt nanoparticle with bigger size is easier to get into the ceria cell and lead to more formation of Pt-O—Ce solution. Then after being treated by H_2/N_2, the oxygen species are consumed and new oxygen vacancies are formed.

3.4. Catalytic activity

The catalytic activity of Pt/CeO_2 with different Pt size were evaluated for toluene oxidation. It could be observed that all samples perform a high activity, which could decompose toluene completely below 180 °C as shown in Fig. 7. In order to compare the activities data easily, the temperatures for 50% and 90% toluene conversion (T_{50} and T_{90}) were calculated and the results were listed in Table 4. It is interesting to observe that the catalytic activities is much dependent on the Pt size. As the Pt size rises from 1.3 to 2.5 nm, the T_{50} and T_{90} decrease first and then increase. The turning point comes with the Pt size of 1.8 nm, and its toluene conversion reaches 50% and 90% at 132 °C and 143 °C, respectively. Moreover, the Arrhenius plots for toluene oxidation over these catalysts were obtained at low conversion (<10%). As shown in Fig. 8, excellent linear relationships (the correlation coefficients were rather close to 1) of ln*r* versus 1000/*T* for all samples were obtained. Table 4 lists the Ea values, and it follows the sequence: Pt/CeO_2-1.8 (56.2 kJ mol^{-1}) < Pt/CeO_2-2.1 (63.9 kJ mol^{-1}) < Pt/CeO_2-2.5 (74.2 kJ mol^{-1}) < Pt/CeO_2-1.5 (79.8 kJ mol^{-1}) < Pt/CeO_2-1.3 (82.9 kJ mol^{-1}). The lower the Ea value, the easier the complete oxidation of toluene, and therefore the higher is the activity of a catalyst. In consistent with the catalytic performance, the results of kinetic investigation confirm that Pt/CeO_2-1.8 sample exhibits the best catalytic performance among all catalysts.

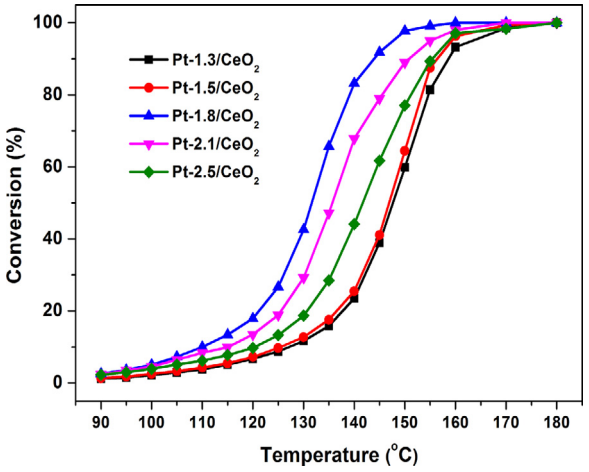

Fig. 7. Conversion of toluene over Pt/CeO_2 catalysts with various Pt size. Catalyst amount: 200 mg; Toluene concentration: 1000 ppm; WHSV: 48,000 ml g^{-1} h^{-1}.

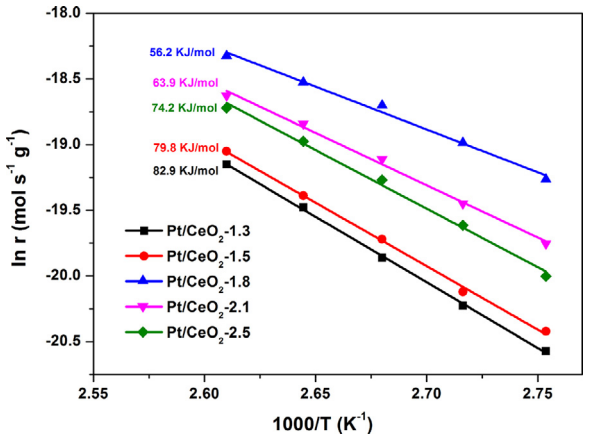

Fig. 8. Arrhenius plots for the oxidation of toluene over Pt/CeO_2 catalysts with various Pt size.

Generally, the catalytic activity for VOCs combustion over Pt-based catalysts is considered to depend on the Pt^0 proportion and Pt dispersion, and higher Pt^0 proportion and Pt dispersion often result in better catalytic performance [43–46]. XPS result above has demonstrated that the Pt^0 proportion of various samples are almost same. Thus, in order to investigate the effect of Pt dispersion on the catalytic reaction, the TOF_{Pt} values had been calculated based on the Pt dispersion according to Eq. (5). And Table 4 lists the TOF_{Pt} values of the samples with various Pt size. It is noticeable that the TOF_{Pt} values with respect to the exposed Pt atom are much different, and a positive correlation exists between TOF_{Pt} value and the Pt size. With the incensement of Pt size, the TOF_{Pt} value becomes bigger from (3.76 ± 0.22) × 10^{-3} s^{-1} to (7.95 ± 0.43) × 10^{-3} s^{-1}. This result

Table 4
Catalytic performances for various catalysts.

Sample	Catalytic activity		E_a(kJ mol^{-1})	TOF_{Pt}[a]($\times 10^{-3}$ s^{-1})	TOF_{ov}[a]($\times 10^{-4}$ s^{-1})	$TOF_{(Pt•ov)}$[a]($\times 10^{-1}$ s^{-1})
	T_{50} (°C)	T_{90} (°C)				
Pt/CeO_2-1.3	148	159	82.9	3.76 ± 0.22	4.89± 0.08	2.69 ± 0.19
Pt/CeO_2-1.5	147	156	79.8	4.66 ± 0.31	4.57± 0.07	2.78 ± 0.21
Pt/CeO_2-1.8	132	143	56.2	6.75 ± 0.35	3.82± 0.02	2.64 ± 0.15
Pt/CeO_2-2.1	136	151	63.9	7.06 ± 0.41	3.11± 0.02	2.64 ± 0.17
Pt/CeO_2-2.5	142	155	74.2	7.95 ± 0.43	2.72± 0.01	2.76 ± 0.16

[a] The TOF values were calculated at 110 °C

indicates that the exposed Pt atom is not the main active site to control the reaction, and another site probably exists to influence the reaction rate.

Previous study demonstrated that the "active support", such as CeO_2, TiO_2 and ZrO_2-Bi_2O_3, could markedly promote the catalytic activity for toluene oxidation through supplying active oxygen species at low temperature [47–49]. And our previous research suggests that oxygen vacancies on Pt/CeO_2 surface are crucial reaction active and play a role in replenishing active oxygen species from gaseous phase and accelerating oxygen cycle for toluene oxidation [50]. As the XPS, Raman and OSC test results prove above, due to various Pt size, the Pt/CeO_2 samples possess different concentration of oxygen vacancy, probably affecting the reaction. So the TOF_{OV} values have been calculated based on concentration of oxygen vacancy, and the data are summarized in Table 4. Unlike TOF_{Pt}, there is a negative correlation between TOF_{OV} value and the Pt size. Pt/CeO_2 sample with bigger Pt size has a smaller TOF_{OV} value. For example, the TOF_{OV} value of Pt/CeO_2-2.5 is $(2.72 \pm 0.01) \times 10^{-4}$ s^{-1} while Pt/CeO_2-1.3 has a biggest value of $(4.89 \pm 0.08) \times 10^{-4}$ s^{-1}. This result indicates that the oxygen vacancies are also not the active to control the rate-determining step.

Further analysis, it is found that activity ordering partly agrees with the trends of the Pt dispersion and concentration of oxygen vacancy. As the Pt size increases from 1.3 nm to 1.8 nm, toluene conversion increases as well as the concentration of oxygen vacancy. On the other hand, from 1.8 nm to 2.5 nm, toluene conversion increases as well as the Pt dispersion. Potentially, it is a comprehensive consideration of both these factors that results in activity ordering. Interestingly, the $TOF_{Pt•OV}$ values that are calculated based on both Pt dispersion and concentration of oxygen vacancy confirm this speculation. As shown in Table 4, the $TOF_{Pt•OV}$ data of various samples are rather close ($(2.69 \pm 0.19) \times 10^{-1}$ s^{-1}, $(2.78 \pm 0.21) \times 10^{-1}$ s^{-1}, $(2.64 \pm 0.15) \times 10^{-1}$ s^{-1}, $(2.64 \pm 0.17) \times 10^{-1}$ s^{-1}, $(2.76 \pm 0.16) \times 10^{-1}$ s^{-1} for Pt/CeO_2-1.3, Pt/CeO_2-1.5, Pt/CeO_2-1.8, Pt/CeO_2-2.1 and Pt/CeO_2-2.5, respectively). This suggests that both the exposed Pt atom and oxygen vacancies on ceria are the active sites to control the reaction rate. Having reported early, for oxidation reaction over NM/CeO_2 (NM: Au, Ag, Pt, etc.) catalysts, the oxidation reaction pathway follows a dual site mechanism [32,50–53]. The metal atom play a role in adsorbing and activating the reactive molecules such as CO and toluene, while the oxygen vacancies on ceria surface is like an oxygen "pump" that transforms gaseous phase oxygen into surface active oxygen species. Back to this work, the Pt/CeO_2 catalyst with smaller Pt size exposes more Pt atoms which could adsorb more toluene molecules and activate them into dehydrogenated intermediates [54,55]. However, the lower concentration of oxygen vacancy means a lower rate of oxygen cycle which could not supply enough active oxygen species to further oxide the intermediates into CO_2 and H_2O, resulting in a lower catalytic activity. Nevertheless, for the Pt/CeO_2 catalyst with bigger Pt size, though more active oxygen species exists on Pt-CeO_2 interface, less dehydrogenated intermediates could be formation due to the limited exposed Pt atoms. Hence the lower rate of toluene activation decreases the reaction rate. As a result, the Pt/CeO_2-1.8 combined both advantages of high Pt dispersion and oxygen vacancy concentration exhibits the best catalytic performance for toluene oxidation, and this is the Pt size effect on the catalytic oxidation of toluene over Pt/CeO_2 catalysts.

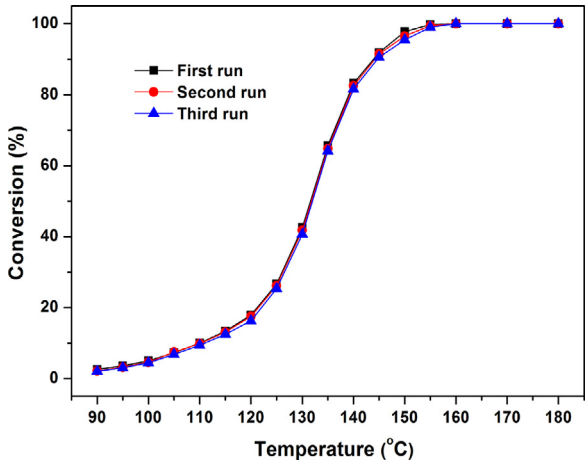

Fig. 9. Conversion of toluene over Pt/CeO_2-1.8 catalyst with three consecutive catalytic runs.

3.5. Stability and H_2O resistance test

Three consecutive catalytic runs and long-term catalytic performance of toluene oxidation over the best-performing catalyst Pt/CeO_2-1.8 were evaluated to investigate the stability of the Pt/CeO_2 catalysts. Fig. 9 shows the toluene conversion curves versus temperature during three consecutive runs. It could be found that the three-run curves overlapped very well, indicating that the Pt/CeO_2-1.8 catalyst was stable after reacting for three times. Long-standing test was set at 155 °C with a higher toluene conversion for the sake of available detection of durability of the catalyst. As shown in Fig. 10, the toluene conversion with 1000 ppm always remains above 99% in 60 h reaction process, exhibiting good reaction stability. As the inlet toluene concentration increase to two times even four times, the toluene conversion wouldn't decline much and could still work effectively for another 60 h. Moreover, with the purpose of further examining if there was any deactivation during the reaction, tolerance activity for toluene oxidation of Pt/CeO_2-1.8 catalyst at lower conversion was tested after the sample has been treated at 300 °C under reactions conditions for 4 h. As Fig. 11 shows, after the heat treatment, the conversion of toluene decreases continuously from 26.5% to 23.5% in beginning 3 h, and then keeps around 23.0% for remaining time. This suggests that the heat treatments would result in the deactivation of catalyst, however, it is slight and about 3%. In a word, all the results suggest that the catalyst of Pt/CeO_2-1.8 is catalytically durable for toluene oxidation.

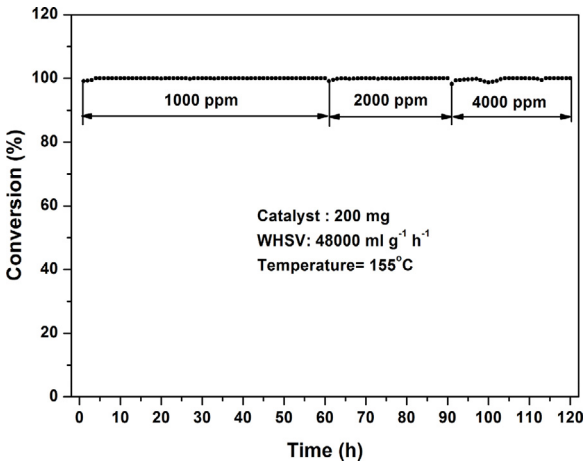

Fig. 10. Reaction stability with time for toluene oxidation over Pt/CeO_2-1.8 catalyst. (Reaction with different various inlet toluene concentration for different time: 1000 ppm for 60 h, 2000 ppm for 30 h, 4000 ppm for 30 h).

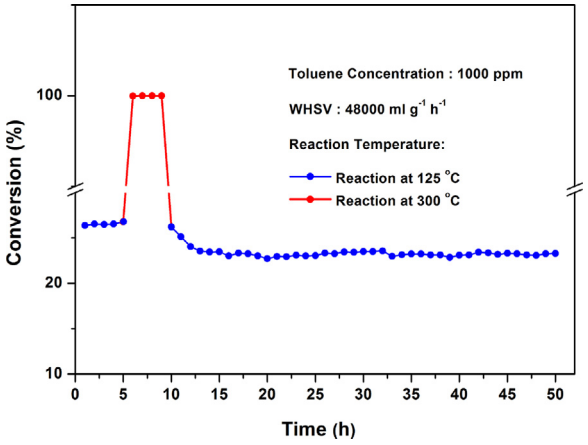

Fig. 11. Tolerance activity for toluene oxidation over Pt/CeO_2-1.8 catalyst at 125 °C.

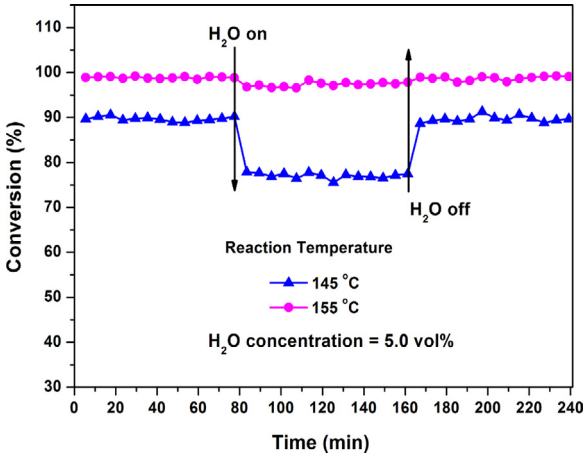

Fig. 12. Effect of water vapour on toluene conversion at different temperature over Pt/CeO_2-1.8 catalyst.

In order to investigate the effect of water vapour on the catalytic performance, we carried out the toluene oxidation experiment in the presence of 5 vol% water vapour over the best-promising Pt/CeO_2-1.8 catalyst at 145 °C and 155 °C. And the results are shown in Fig. 12, it is found that the incorporation of water vapour at 145 °C would decrease the toluene conversion about 15%. When the water was cut off, the toluene conversion was almost restored to the original value. The activity deactivation caused by the water vapour probably due to the competitive adsorption of water and toluene as well as oxygen molecules on catalyst surface [56]. When temperature is at 155 °C, no significant loss in catalytic activity is observed, indicating the addition of 5 vol% water vapour would not affect the combustion of toluene if the temperature is higher. Rather than on the precious metal, the water molecule would like to adsorb on the metal oxide support. At a relative higher temperature, the oxygen vacancies on CeO_2 would be more facile in the activation of oxygen molecules, where the adsorption of oxygen is stronger than water vapour [57].

4. Conclusions

In summary, a series of size-controllable Pt nanoparticles has been fabricated through a glycol reduction method and then supported on CeO_2 nanorod by adsorption. The Pt/CeO_2 catalysts exhibit a significantly Pt-size-dependent catalytic activity toward toluene oxidation. The Pt/CeO_2-1.8 sample performs the best catalytic activity (T_{50} = 132 °C, T_{90} = 143 °C) due to the balance of both Pt dispersion and oxygen vacancy concentration. Three types of TOFs results show that the TOF_{Pt} and TOF_{OV} values are diverse while the $TOF_{Pt•OV}$ are almost identical, indicating that both the exposed Pt atom and oxygen vacancies on ceria surface are the active site to control the reaction rate. Furthermore, the most active Pt/CeO_2 catalyst proved to be perfectly stable during the toluene oxidation. The addition of 5 vol% water vapour to the feed would temporarily inhibit the catalyst activity, however, the increase in the reaction temperature, above 155 °C, will eliminate the effect. These results would be helpful for understanding the Pt size effect on the toluene catalytic oxidation and for developing highly active catalyst system.

Acknowledgements

This work is financially supported by the National Natural Science Foundation of China (No. 51378218, 51108187, 21207039 and 50978103), the Fundamental Research Funds for the Central Universities (Grant No. 2014A030310431), and Natural Science Foundation of Guangdong Province, China (Grant No.2016A030311003).

Appendix A. Supplementary data

Supplementary data associated with this article can be found, in the online version, at http://dx.doi.org/10.1016/j.apcatb.2017.07.048.

References

[1] A. Rokicińska, P. Natkański, B. Dudek, M. Drozdek, L. Lityńska Dobrzyńska, P. Kuśtrowski, Appl. Catal. B: Environ. 195 (2016) 59–68.
[2] M. Alifanti, M. Florea, V.I. Pârvulescu, Appl. Catal. B: Environ. 70 (2007) 400–405.
[3] Q. Huang, S. Zuo, R. Zhou, Appl. Catal. B: Environ. 95 (2010) 327–334.
[4] W. Tan, J. Deng, S. Xie, H. Yang, Y. Jiang, G. Guo, H. Dai, Nanoscale 7 (2015) 8510–8523.
[5] Z. Qu, K. Gao, Q. Fu, Y. Qin, Catal. Commun. 52 (2014) 31–35.
[6] L.Y. Lin, C. Wang, H. Bai, Chem. Eng. J. 264 (2015) 835–844.
[7] H. Huang, Y. Xu, Q. Feng, D.Y.C. Catal. Sci. Technol. 5 (2015) 2649–2669.
[8] S. Xie, Y. Liu, J. Deng, X. Zhao, J. Yang, K. Zhang, Z. Han, H. Arandiyan, H. Dai, Appl. Catal. B: Environ. 206 (2017) 221–232.
[9] C. Chen, J. Zhu, F. Chen, X. Meng, X. Zheng, X. Gao, F.-S. Xiao, Appl. Catal. B: Environ. 140-141 (2013) 199–205.
[10] S. Su, C. Zhang, L. Yuwen, X. Liu, L. Wang, C. Fan, L. Wang, Nanoscale 8 (2015) 602–608.
[11] R.M.R. Hyunjoon Song, James D. Hoefelmeyer, Russell Komor, Krisztian Niesz, Michael Grass, Peidong Yang, Gabor A. Somorjai, J. Am. Chem. Soc. 128 (2009) 3027–3037.

[12] V.V. Pushkarev, K. An, S. Alayoglu, S.K. Beaumont, G.A. Somorjai, J. Catal. 292 (2012) 64–72.
[13] M. Nesselberger, M. Roefzaad, R.F. Hamou, P.U. Biedermann, F.F. Schweinberger, S. Kunz, K. Schloegl, G.K. Wiberg, S. Ashton, U. Heiz, K.J. Mayrhofer, M. Arenz, Nature Mater. 12 (2013) 919–924.
[14] K. Kon, S.M.A. Hakim Siddiki, K. i. Shimizu, J. Catal. 304 (2013) 63–71.
[15] K.B.K. Jung Eun Park, Young-A. Kim, Kwang Sup Song, Eun Duck Park, Catal. Lett. 143 (2013) 1132–1138.
[16] Y. Li, F. Zaera, J. Catal. 326 (2015) 116–126.
[17] C. Chen, F. Chen, L. Zhang, S. Pan, C. Bian, X. Zheng, X. Meng, F.S. Xiao, Chem. Commun. 51 (2015) 5936–5938.
[18] M. Cargnello, V.V. Doan Nguyen, T.R. Gordon, R.E. Diaz, E.A. Stach, R.J. Gorte, P. Fornasiero, C.B. Murray, Science 341 (2013) 771–773.
[19] S.L.N. An, P.N. Duchesne, P. Wu, W. Zhang, J. Phys. Chem. C 117 (2013) 21254–21262.
[20] N. Li, Q.Y. Chen, L.F. Luo, W.X. Huang, M.F. Luo, G.S. Hu, J.Q. Lu, Appl. Catal. B: Environ. 142-143 (2013) 523–532.
[21] H.H. Liu, Y. Wang, A.P. Jia, S.Y. Wang, M.F. Luo, J.Q. Lu, Appl. Surf. Sci. 314 (2014) 725–734.
[22] Y. Liao, L. He, C. Man, L. Chen, M. Fu, J. Wu, D. Ye, B. Chem, Eng. J. 256 (2014) 439–447.
[23] F. Wang, C. Li, X. Zhang, M. Wei, D.G. Evans, X. Duan, J. Catal. 329 (2015) 177–186.
[24] T. Désaunay, G. Bonura, V. Chiodo, S. Freni, J.P. Couzinié, J. Bourgon, A. Ringuedé, F. Labat, C. Adamo, M. Cassir, J. Catal. 297 (2013) 193–201.
[25] H. Huang, Q. Dai, X. Wang, Appl. Catal. B: Environ. 158-159 (2014) 96–105.
[26] T.H. Seiichiro Imamura, Yoshio Saito, Hirofumi Aritani, Catal. Today 50 (1999) 369–380.
[27] J. Xu, X.C. Xu, L. Ouyang, X.J. Yang, W. Mao, J. Su, Y.F. Han, J. Catal. 287 (2012) 114–123.
[28] C. Chen, X. Wang, J. Zhang, S. Pan, C. Bian, L. Wang, F. Chen, X. Meng, X. Zheng, X. Gao, F.S. Xiao, Cataly. Lett. 144 (2014) 1851–1859.
[29] K.B.M. Romeo, J. El Fallah, F. Le Normand, L. Hilaire, Surf. Interface Anal. 20 (1993) 508–512.
[30] J.M. López, A.L. Gilbank, T. García, B. Solsona, S. Agouram, L. Torrente Murciano, Appl. Catal. B: Environ. 174-175 (2015) 403–412.
[31] P. Reys, G. Pecchi, M. Morales, J.L.G. Fierro, Appl. Catal. A: Gene. 163 (1997) 145–152.
[32] S.K. Meher, M. Cargnello, H. Troiani, T. Montini, G.R. Rao, P. Fornasiero, Appl. Catal. B: Environ. 130-131 (2013) 121–131.
[33] B. Murugan, A.V. Ramaswamy, J. Am. Chem. Soc. 129 (2007) 3062–3063.
[34] F.C. Calaza, Y. Xu, D.R. Mullins, S.H. Overbury, J. Am. Chem. Soc. 134 (2012) 18034–18045.
[35] A. Aranda, S. Agouram, J.M. López, A.M. Mastral, D.R. Sellick, B. Solsona, S.H. Taylor, T. García, Appl. Catal. B: Environ. 127 (2012) 77–88.
[36] J. Paier, C. Penschke, J. Sauer, Chem. Rev. 113 (2013) 3949–3985.
[37] Z. Wu, M. Li, J. Howe, H.M. Meyer, S.H. Overbury, Langmuir 26 (2010) 16595–16606.
[38] S. Chang, M. Li, Q. Hua, L. Zhang, Y. Ma, B. Ye, W. Huang, J. Catal. 293 (2012) 195–204.
[39] S. Agarwal, X. Zhu, E.J.M. Hensen, L. Lefferts, B.L. Mojet, J. Phys. Chem. C 118 (2014) 4131–4142.
[40] C. Hess, Top. Catal. 56 (2013) 1593–1600.
[41] X. Du, D. Zhang, L. Shi, R. Gao, J. Zhang, J. Phys. Chem. C 116 (2012) 10009–10016.
[42] L. Liu, Z. Yao, Y. Deng, F. Gao, B. Liu, L. Dong, ChemCatChem 3 (2011) 978–989.
[43] K. Bendahou, L. Cherif, S. Siffert, H.L. Tidahy, H. Benaïssa, A. Aboukaïs, Appl.Catal. A: Gen. 351 (2008) 82–87.
[44] T.Y.C. Jeffrey, C.S. Wu, Catal. Today 44 (1998) 111–118.
[45] V.P. Santos, S.A.C. Carabineiro, P.B. Tavares, M.F.R. Pereira, J.J.M. Órfão, J.L. Figueiredo, Appl. Catal. B: Environ. 99 (2010) 198–205.
[46] L.F. Liotta, Appl. Catal. B: Environ. 100 (2010) 403–412.
[47] H.A.E. Dole, R.J. Isaifan, F.M. Sapountzi, L. Lizarraga, D. Aubert, A. Princivalle, P. Vernoux, E.A. Baranova, Catal. Lett. 143 (2013) 996–1002.
[48] T. Masui, H. Imadzu, N. Matsuyama, N. Imanaka, J. Hazard. Mater. 176 (2010) 1106–1109.
[49] S.M. Saqer, D.I. Kondarides, X.E. Verykios, Top. Catal. 52 (2009) 517–527.
[50] R. Peng, X. Sun, S. Li, L. Chen, M. Fu, J. Wu, D. Ye, Chem. Eng. J. 306 (2016) 1234–1246.
[51] H.Y. Kim, H.M. Lee, G. Henkelman, J. Am. Chem. Soc. 134 (2012) 1560–1570.
[52] N. Ta, J.J. Liu, S. Chenna, P.A. Crozier, Y. Li, A. Chen, W. Shen, J. Am. Chem. Soc. 134 (2012) 20585–20588.
[53] A.D. Allian, K. Takanabe, K.L. Fujdala, X. Hao, T.J. Truex, J. Cai, C. Buda, M. Neurock, E. Iglesia, J. Am. Chem. Soc. 133 (2011) 4498–4517.
[54] D.J.B. Anderson, L. Marsh, Daniel A. Fischer, John L. Gland, J. Phys. Chem. B 108 (2004) 605–611.
[55] Y.T. Lai, T.C. Chen, Y.K. Lan, B.S. Chen, J.H. You, C.M. Yang, N.C. Lai, J.H. Wu, C.S. Chen, ACS Catal. 4 (2014) 3824–3836.
[56] S. Xie, H. Dai, J. Deng, Y. Liu, H. Yang, Y. Jiang, W. Tan, A. Ao, G. Guo, Nanoscale 5 (2013) 11207–11219.
[57] Y. Liu, H. Dai, J. Deng, S. Xie, H. Yang, W. Tan, W. Han, Y. Jiang, G. Guo, J. Catal. 309 (2014) 408–418.